Welding in the World (2022) 66:753–766
https://doi.org/10.1007/s40194-021-01240-x

RESEARCH PAPER

Determination of notch factors for transverse non-load carrying stiffeners based on numerical analysis and metamodeling

Josef Neuhäusler[1] · **Klemens Rother**[1]

Received: 3 August 2021 / Accepted: 16 December 2021 / Published online: 21 January 2022

Abstract

Stress concentration factors (SCFs) at weld toes and weld roots as required for the effective notch stress concept (see [1, 2]) are usually computed using finite element analysis (FEA) which requires a certain amount of effort for model generation, the solving process, and postprocessing. Regression functions of many FEAs within given parameter bounds provide the possibility of a fast prediction of SCFs. This paper provides new and accurate regression formulae for the estimation of notch stresses at idealized weld geometries on the basis of multiple linear-elastic FEAs for the transverse stiffener (non-load carrying T-joint) under tension and bending of the load carrying slab. Regression of sampled finite element results has been performed using (a) second-order polynomial regression with coupling terms (PRC) and (b) artificial neural networks (ANN). The presented formulae are compared with several existing estimations of stress concentration factors. The new methods appear to show a higher quality of prognosis as well as apply to significant larger ranges of the geometrical parameters of the weld joint. The formulae presented here for the transverse stiffener add another welded joint to a series of similar surrogate models presented from Munich University of Applied Sciences in earlier publications and made available for use by the web-based tool *SCF-Predictor*.

IIW-Thesaurus keywords Elastic analysis · Finite element analysis · Surrogate models · Sampling · Notches · Transverse stiffeners

Nomenclature

Symbols, abbreviations

ANN [-]	Artificial neural network
α [°]	Flank angle
$\boldsymbol{b_i}$ [-]	Bias vectors for artificial neural networks
c_k [-]	Scalar multiplication parameter for the PRC method
d [mm]	Total model depth
E [MPa]	Modulus of elasticity
err_{rel} [%]	Relative error
FEA [-]	Finite element analysis
F [N]	Force
f_a [-]	Ratio of weld seam width to sheet thickness
f_k [-]	Value of geometric multiplication parameter for the PRC method
$\boldsymbol{g}$ [-]	Input vector for the ANN method
K_f [-]	Fatigue notch factor
K_t [-]	Stress concentration factor
$K_{t,\,EST}$ [-]	Stress concentration factor, estimated
$K_{t,\,FEM}$ [-]	Stress concentration factor, calculated by FEM
$\boldsymbol{k_t}$ [-]	Stress concentration output vector of the ANN method
$K_{t,\,ANN}$ [-]	Stress concentration factor of the ANN method
$K_{t,\,PRC}$ [-]	Stress concentration factor of the PRC method
$K_{t,\,TSUJ}$ [-]	Stress concentration factor of Tsuji's method
$K_{t,\,MONA/BREN/HELL}$ [-]	Stress concentration factor of Monahan's or Brennan's or Hellier's method

Recommended for publication by Commission XIII - Fatigue of Welded Components and Structures

✉ Josef Neuhäusler
josef.neuhaeusler@hm.edu

[1] Department Mechanical, Automotive and Aerospace Engineering, Institute for Material and Building Research, Munich University of Applied Sciences, Dachauerstr. 98b, 80335 Munich, Germany

K_w [-]	Ratio of notch stress to structural stress
$K_{w,\,min}$ [-]	Minimum ratio of notch stress to structural stress
L [mm]	Length of sheet
M [N/mm]	Moment
ν [-]	Poisson ratio
$\boldsymbol{\Phi_i}$ [-]	Artificial neural network layer potential
PRC [-]	Polynomial regression with coupling terms
ρ [mm]	Notch radius
S_b [MPa]	Nominal bending stress
S_t [MPa]	Nominal tension stress
σ_n [MPa]	Notch stress
σ_s [MPa]	Structural stress
t_1, t_2 [mm]	Sheet thicknesses
$\boldsymbol{W_i}$ [-]	Weight matrices of artificial neural networks
$\boldsymbol{x_{i,gain}}$ [-]	Gain input vector for artificial neural networks
$\boldsymbol{x_{i,offset}}$ [-]	Offset input vector for artificial neural networks
$\boldsymbol{y_{o,gain}}$ [-]	Gain output vector of artificial neural networks
$\boldsymbol{y_{o,offset}}$ [-]	Offset output vector of artificial neural networks

Indices, superscripts

b, bend	Bending
t, tens	Tension
f. p.	Full penetration
k	PRC method index
toe	toe

1 Introduction

The effective notch stress approach according to IIW recommendations [1] is based on the idealization of weld toes and weld roots using a fictitious radius $\rho = 1$ mm. The DVS Merkblatt 0905 [2] suggests even smaller radii of $\rho = 0.3$ mm and $\rho = 0.05$ mm depending on the sheet thickness accompanied by associated FAT classes. Application of the effective notch stress approach for different fictitious radii can be found in [3]. There have been several investigations on the effective notch stress approach using these three distinct radii to design against fatigue of welded joints made of different materials such as magnesium alloys [4, 5]. A comparison of the effective notch stress approach using the three radii with the well-known structural and nominal stress approaches can be found in [6]. Sizing recommendations of this radius are based on the thickness of the weld leg length and sheet thickness based on accuracy and computational efficiency, as can be seen in [2]. Depending on the selected size of the radius and group of material, FAT classes have been derived by backward calculations from experimentally obtained life data using this concept conforming modeling rule for the fictitious radius ρ. This way, the theoretical notch factor K_t represents already the fatigue notch factor K_f. The notch stress concept as described in [1, 2] has been originally proposed by Seeger et al. [7] which was motivated on early works of Radaj [8] and Neuber [9].

Renken et al. [10] recently have shown an application of the notch stress concept for the analysis of scanned weld topographies and distributions of local SCFs. There exist several other contributions where weld topographies have been scanned and analyzed numerically. Alam et al. [11] investigated eccentric fillet joints in such way, while Liinalampi et al. [12] analyzed laser-hybrid welds with thin plates in a similar fashion. Ottersböck et al. [13] characterized actual weld geometry and stress concentrations of butt welds and compared numerical results with approximation solutions.

The goal of this paper is to provide computational efficient estimations for SCFs of transverse non-load carrying stiffeners for three distinct weld toe radii $\rho = 1$ mm, $\rho = 0.3$ mm, and $\rho = 0.05$ mm for supporting fatigue evaluations according to [2, 3]. Two new surrogate models based on a large amount of samples processed using FEA of transverse non-load carrying stiffeners with varying geometrical parameters of flank angle α, reference radius ρ, sheet thicknesses t_1, t_2, and weld seam thickness a are provided. The paper extends an already investigated and published collection of the joint types (a) cruciform joints [14], (b) butt joints [15], and (c) load carrying T-joints [16].

The proposed estimations are compared to existing equations by Tsuji [17], Monahan [18], Brennan et al. [19], and Hellier et al. [20]. Similar analyses using artificial neural networks for nonlinear regression demonstrating a very good quality of prognosis have been published by Dabiri et al. [21]. The latter solution was done using a smaller application range of the parameters and only for full penetration welds. Because the ANN of this group was not published, a direct comparison with the proposed methods in the present paper was not possible. Since the application of ANN and advanced PRC for SCF estimation is a relatively new approach, these methods were chosen for this investigation. The methods appear to significantly reduce scatter in predicting SCFs for large ranges of the parameters considered.

2 Numerical simulation of welded T-joints

The numerical models of the transverse non-load carrying stiffeners cover the geometrical parameters given in Table 1 and 2 with the respective ranges of variables for sampling.

Table 1 Parameter ranges of numerical model

Parameter		Range
Flank angle [°]	α	[110; 160]
Reference radius [*mm*]	ρ	See Table 2
Sheet thickness [*mm*]	t_1, t_2	See Table 2
Weld seam thickness	$a = f_a t_1$	$[0.1t_1; 0.9t_1]$
Length of the base plate [mm]	L_1	150
Length of the attachment [mm]	L_2	50

Table 2 Parameter ranges for space filling Latin hypercube samplings

Subsystem	ρ [*mm*]	t_1, t_2 [mm]	α [°]	$a = f_a t_1$[*mm*]	Samples
1	1.0	[5; 50]	[110; 160]	$[0.1t_1; 0.9t_1]$	1599
2	0.3	[1.5; 20]	[110; 160]	$[0.1t_1; 0.9t_1]$	1519
3	0.05	[0.25; 5]	[110; 160]	$[0.1t_1; 0.9t_1]$	1461

Axial or angular misalignment are not covered in the finite element models. In case misalignments are present, they have to be covered as secondary effects in the SCF K_t as presented in [1] or by reducing the allowable stress.

2.1 Parametrization

The linear-elastic FEAs were performed in ANSYS Mechanical™ 18.1[1] according to Fig. 1 and Table 1 and 2. The models are loaded by tension and bending (see Fig. 2). For each load case, full penetration welds have been considered.

The following assumptions apply to the finite element models:

- No axial or angular misalignment is covered.
- The weld seam flank is modeled by a straight line.
- Quadratic PLANE183 elements with plane strain condition.
- Constant parameters for linear elastic material:
  - Modulus of elasticity $E = 210 GPa$
  - Poisson ratio $\nu = 0.3$
- Uniform tension or bending nominal stress of $S_t = S_b = 1 MPa$.
- Evaluation of maximum principal stress σ_1 at the weld toe.
- The SCF $K_t = \frac{\sigma_1}{S_{t/b}}$ is defined as the ratio of maximum principal stress σ_1 at the weld toe to uniform tension or bending nominal stress of $S_t = S_b = 1 MPa$.

DVS Merkblatt 0905 [2] addresses three different reference radii $\rho = 1.0$ mm/0.3 mm/0.05 mm depending on the sheet thickness. Hence, the design space is additionally separated into a subsystem for each reference radius (see Table 2). Note that the equations presented in this paper provide SCFs based on maximum principal stress. Similar formulas could be derived on the basis of v. Mises equivalent stress in the notch radius. In that case, Sonsino [22] suggests different FAT values for fatigue evaluation based on v. Mises equivalent stress values.

2.2 Finite element modeling and sampling

The finite element models are meshed with PLANE183 elements of quadratic order and with plane strain condition. The areas around the weld toes are mapped meshed with quadrilateral elements with element lengths of $0.05 \cdot \rho$ in the notch up to a depth of $0.4 \cdot \rho$. An exemplary finite element mesh is shown in Fig. 3. More detailed information on numerical modeling can be found in [14].

For each subsystem in Table 2, a space filling Latin hypercube sampling was created with optiSLang® 7.2.0[2]. In total, 4579 samples were successfully simulated.

Further information on sampling and modeling can be found in [14, 15].

The parameter ranges in Table 2 have been chosen. They cover all and beyond of the parameter ranges of the older equations from other authors as presented in Section 3. These parameters are typical for arc welded transverse non-load carrying stiffeners.

3 Known methods of notch factor estimation of T-joints

This section shows already published methods for the estimation of SCFs. Their predictive quality will be compared with the newly proposed methods using polynomial regression with coupling terms (PRC) and artificial neural networks (ANN). Most of the older equations presented in this section are of simpler form than the presented solutions using PRC and ANN. Because of the more complex form of the new approaches, the models PRC and ANN basically have a better adaptability to the finite element-based data points which leads to smaller errors in predicting SCFs of geometry combinations within the allowable parameter ranges.

[1] ANSYS Mechanical™ is a trademark of ANSYS, Inc., Canonsburg, PA, USA (see http://www.ansys.com).

[2] optiSLang® is a trademark of Dynardo GmbH, Weimar, Germany (an ANSYS, Inc. company) (see https://www.dynardo.de/software/optislang.hmtl).

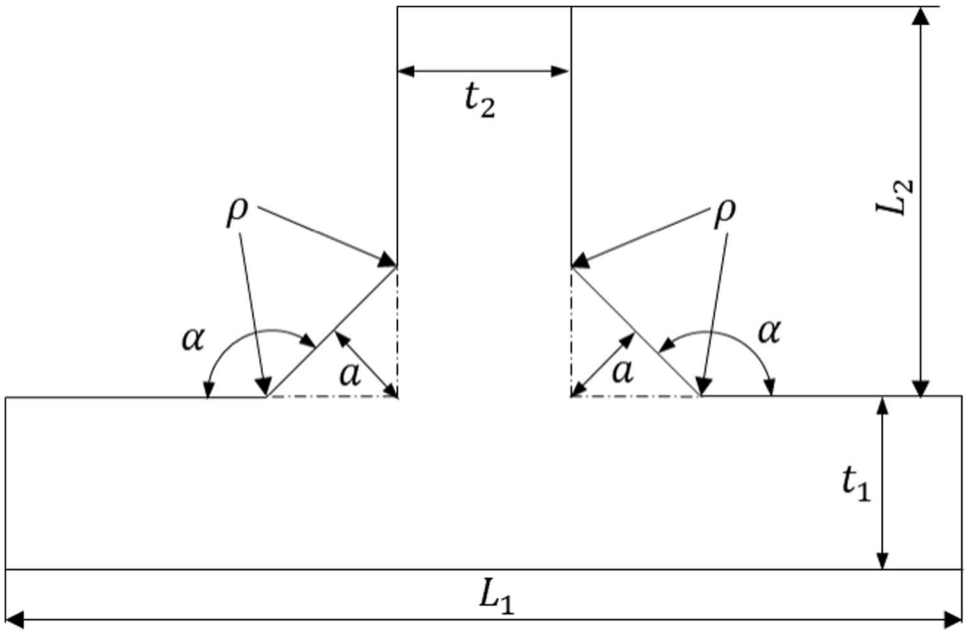

Fig. 1 Parametrized geometry of the T-joint with full penetration

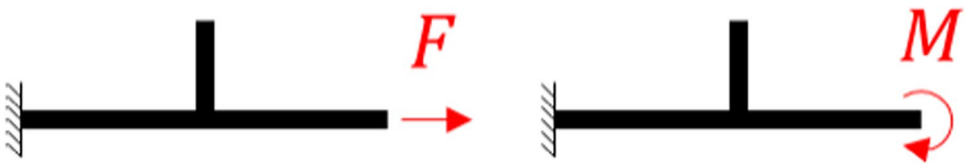

Fig. 2 Load cases 1 (tension) (left) and 2 (bending) (right)

3.1 Method by Tsuji

Tsuji [17] in 1990 published regression-based equations for notch factors of transverse non-load carrying stiffeners subjected to tension and bending loading. The equations were derived on the basis of multiple boundary element method calculations. The range of validity is not explicitly given for the Tsuji's method given in Table 3.

3.2 Method by Monahan

Monahan [18] proposed two formulae for SCFs at the weld toe. Their range of validity is restricted to $120° < \alpha < 150°$ and $0.02 < \rho/t_1 < 0.066$. The formulae are given in Table 4.

3.3 Method by Brennan

Brennan et al. [19] derived regression equations for SCFs on the basis of 80 different weld toe T-butt geometries which are displayed in Table 5. The calculations were performed using linear elastic FEA and plane stress condition. The geometry validity limits are $120° < \alpha < 150°$, $0.01 < \rho/t_1 < 0.066$, and $0.3 < L/t_1 < 4.0$ where L is the attachment width.

3.4 Method by Hellier

Hellier et al. [20] published equations for SCFs of tension loaded T-joints which have a similar structure like the

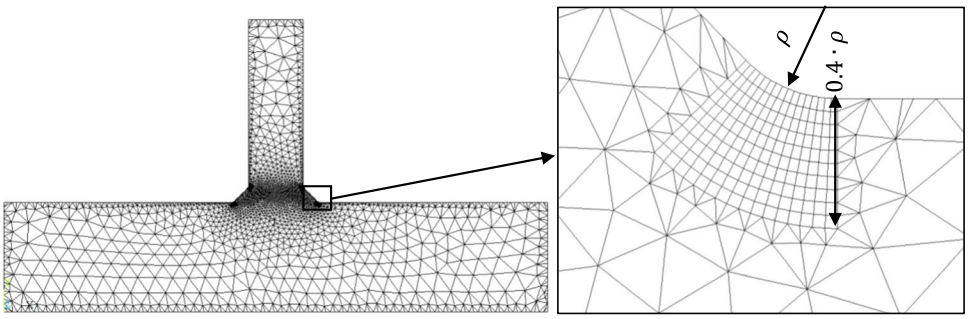

Fig. 3 Complete finite element mesh (left) and mesh refinement in the notch at weld toes (right)

Table 3 Method by Tsuji

Position	Loading	Equation	
Weld toe	Tension	$K_{t,\,TSUJ,\,tens} = 1 + 1.015Q^{0.446} f(180^\circ - \alpha)$	(1)
		$f(180^\circ - \alpha) = \dfrac{1 - e^{-0.9\left(\frac{(180^\circ-\alpha)\pi}{180^\circ}\right)\sqrt{\frac{t_1 + \frac{t_1 f_a}{\sin\left(\frac{\pi}{2} - \frac{(180^\circ-\alpha)\pi}{180^\circ}\right)}}{2\frac{t_1 f_a}{\sin\left(\frac{\pi}{2} - \frac{(180^\circ-\alpha)\pi}{180^\circ}\right)}}}}}{1 - e^{-0.9\left(\frac{\pi}{2}\right)\sqrt{\frac{t_1 + \frac{t_1 f_a}{\sin\left(\frac{\pi}{2} - \frac{(180^\circ-\alpha)\pi}{180^\circ}\right)}}{2\frac{t_1 f_a}{\sin\left(\frac{\pi}{2} - \frac{(180^\circ-\alpha)\pi}{180^\circ}\right)}}}}}$	
		$Q = \dfrac{1}{2.8\left(\frac{t_1 + \frac{t_1 f_a}{\sin\left(\frac{\pi}{2} - \frac{(180^\circ-\alpha)\pi}{180^\circ}\right)}}{t_1}\right) - 2}\left(\dfrac{\frac{t_1 f_a}{\sin\left(\frac{\pi}{2} - \frac{(180^\circ-\alpha)\pi}{180^\circ}\right)}}{\rho}\right)$	
	Bending	$K_{t,TSUJ,bend} = 1 + \left(0.629 + 0.058\ln\left(\dfrac{t_2 + 2\frac{t_1 f_a}{\sin\left(\frac{(180^\circ-\alpha)\pi}{180^\circ}\right)}}{t_1}\right)\right)\left(\dfrac{\rho}{t_1}\right)^{-0.431}\tanh\left(\dfrac{6\frac{t_1 f_a}{\sin\left(\frac{\pi}{2} - \frac{(180^\circ-\alpha)\pi}{180^\circ}\right)}}{t_1}\right) f(180^\circ - \alpha)$	(2)

Table 4 Method by Monahan

Position	Loading	Equation	
Weld toe	Tension	$K_{t,MONA,tens} = 1 + 0.388\left(\frac{(180^\circ-\alpha)\pi}{180^\circ}\right)^{0.37}\left(\frac{\rho}{t_1}\right)^{-0.454}$	(3)
	Bending	$K_{t,MONA,bend} = 1 + 0.512\left(\frac{(180^\circ-\alpha)\pi}{180^\circ}\right)^{0.572}\left(\frac{\rho}{t_1}\right)^{-0.469}$	(4)

Table 5 Method by Brennan et al.

Position	Loading	Equation	
		$L = t_2 + 2\dfrac{t_1 f_a}{\sin\left(\frac{(180^\circ-\alpha)}{180^\circ}\pi\right)}\gamma = \frac{(180^\circ-\alpha)\pi}{180^\circ}$	
Weld toe (simplified)	Tension	$K_{t,BREN,tens} = 1.027 + 0.271\gamma^{0.261}\left(\frac{\rho}{t_1}\right)^{-0.47}\left(\frac{L}{t_1}\right)^{0.183}$	(5)
	Bending	$K_{t,BREN,bend} = 1.01 + 0.344\gamma^{0.336}\left(\frac{\rho}{t_1}\right)^{-0.468}\left(\frac{L}{t_1}\right)^{0.233}$	(6)
Weld toe (full)	Tension	$K_{t,BREN,tens} = 1.1 + 0.067\alpha - 0.25\left(\frac{\rho}{t_1}\right) - 0.04\left(\frac{L}{t_1}\right) + 0.003\alpha^2 - 12\left(\frac{\rho}{t_1}\right)^2 - 0.014\left(\frac{L}{t_1}\right)^2 + 0.0164\alpha^3 - 0.0005\left(\frac{L}{t_1}\right)^3 + 0.00004\left(\frac{L}{t_1}\right)^4 - 0.3\alpha\left(\frac{\rho}{t_1}\right) - 0.023\alpha\left(\frac{L}{t_1}\right) + 0.91\left(\frac{\rho}{t_1}\right)\left(\frac{L}{t_1}\right) - 8.3\alpha^2\left(\frac{\rho}{t_1}\right) + 0.255\alpha^2\left(\frac{L}{t_1}\right) + 100.5\alpha\left(\frac{\rho}{t_1}\right)^2 - 0.0792\alpha\left(\frac{L}{t_1}\right)^2 - 37.5\left(\frac{\rho}{t_1}\right)^2\left(\frac{L}{t_1}\right) + 0.908\left(\frac{\rho}{t_1}\right)\left(\frac{L}{t_1}\right)^2 + 0.27\alpha^{0.19}\left(\frac{\rho}{t_1}\right)^{-0.74}\left(\frac{L}{t_1}\right)^{0.25}$	(7)
	Bending	$K_{t,BREN,bend} = 1.14 + 0.13\alpha - 0.67\left(\frac{\rho}{t_1}\right) - 0.083\left(\frac{L}{t_1}\right) + 0.08\alpha^2 + 28\left(\frac{\rho}{t_1}\right)^2 - 0.02\left(\frac{L}{t_1}\right)^2 + 0.01\alpha^3 - 0.0005\left(\frac{L}{t_1}\right)^3 - 0.00002\left(\frac{L}{t_1}\right)^4 - 4.3\alpha\left(\frac{\rho}{t_1}\right) - 0.09\alpha\left(\frac{L}{t_1}\right) - 1.03\left(\frac{\rho}{t_1}\right)\left(\frac{L}{t_1}\right) - 13.7\alpha^2\left(\frac{\rho}{t_1}\right) + 0.443\alpha^2\left(\frac{L}{t_1}\right) + 150\alpha\left(\frac{\rho}{t_1}\right)^2 - 0.13\alpha\left(\frac{L}{t_1}\right)^2 - 62\left(\frac{\rho}{t_1}\right)^2\left(\frac{L}{t_1}\right) + 1.53\left(\frac{\rho}{t_1}\right)\left(\frac{L}{t_1}\right)^2 + 0.005\alpha^3\left(\frac{L}{t_1}\right) - 30\alpha\left(\frac{\rho}{t_1}\right)^3 + 3.57\alpha\left(\frac{\rho}{t_1}\right)\left(\frac{L}{t_1}\right) + 5\alpha\left(\frac{\rho}{t_1}\right)^2\left(\frac{L}{t_1}\right) + 0.35\alpha^{0.26}\left(\frac{\rho}{t_1}\right)^{-0.468}\left(\frac{L}{t_1}\right)^{0.3}$	(8)

equations by Brennan. In fact, the "simplified" version of the equation is exactly the same. Only the "full equation" differs from the one by Brennan, see Table 6. The range of validity is also similar to the ones given by Brennan.

Table 6 Method by Hellier

Position	Loading	Equation
		$L = t_2 + 2\frac{t_1 f_a}{\sin\left(\frac{(180°-\alpha)}{180°}\pi\right)} \gamma = \frac{(180°-\alpha)\pi}{180°}$
Weld toe (simplified)	Tension	$K_{t,HELL,tens} = 1.027 + 0.271\gamma^{0.261}\left(\frac{\rho}{t_1}\right)^{-0.47}\left(\frac{L}{t_1}\right)^{0.183}$ (9)
Weld toe (full)	Tension	$K_{t,HELL,tens} = 0.889 - 0.302\alpha + 3.44\left(\frac{\rho}{t1}\right) + 0.529\left(\frac{L}{t1}\right) + 0.012\alpha^2$ (10) $+ 104\left(\frac{\rho}{t_1}\right)^2 - 0.633\left(\frac{L}{t1}\right)^2 - 0.614\alpha^3 + 0.18\left(\frac{L}{t1}\right)^3 - 0.018\left(\frac{L}{t1}\right)^4 - 35.5\alpha\left(\frac{\rho}{t1}\right) - 0.153\alpha\left(\frac{L}{t1}\right)$ $+ 4.38\left(\frac{\rho}{t1}\right)\left(\frac{L}{t1}\right) + 30.6\alpha^2\left(\frac{\rho}{t1}\right) - 0.219\alpha^2\left(\frac{L}{t1}\right) - 64.3\alpha\left(\frac{\rho}{t1}\right)^2 + 0.041\alpha\left(\frac{L}{t1}\right)^2 - 54.5\left(\frac{\rho}{t1}\right)^2\left(\frac{L}{t1}\right)$ $+ 0.595\left(\frac{\rho}{t1}\right)\left(\frac{L}{t1}\right)^2 + \alpha^{0.68}\left(\frac{\rho}{t1}\right)^{-0.299}\left(\frac{L}{t1}\right)^{0.263}$

4 New methods of notch factor determination

In this section, the two methods for the derivation of estimation formulae for SCFs are presented. The input values for the estimations shall be the geometrical parameters according to Table 1 and 2, whereas the output value is a single scalar value, the SCF based on the maximum principle stress σ_1.

4.1 Polynomial regression with coupling terms (PRC method)

The polynomial regression of quadratic order with coupling terms is carried out in optiSLang® 7.2.0. Equation (11) shows how the SCF is calculated with the respective factors $c_k \bullet f_k(t_1, \alpha, f_a)$ according to Table 12. The restrictions for the equation can be found in Table 7.

The nomenclature of the SCF for each reference radius and loading type is determined in Table 8.

$$K_{t,PRC} = \sum_{k=1}^{10} c_k \bullet f_k\left(t_1, \alpha, f_a\right) \tag{11}$$

The three parameters (t_1, α, f_a) yield a maximum of 10 terms for the estimation of a SCF. The 10 terms result from the three parameters, their squares, each combination of two parameters, and one fixed term. In case one of these terms does not significantly affect the SCF, they are filtered out by optiSLang. The default filter settings have been used.

Table 7 Restrictions of the PRC method

Parameter combination	t_1, t_2 [mm]	$\frac{t_1}{t_2}$ or $\frac{t_2}{t_1}$	f_a
Restriction	5…50 for $\rho = 1.00mm$	$\frac{1}{3} < \frac{t_{1/2}}{t_{2/1}} < 3$	0.1…0.9
	1.5…20 for $\rho = 0.30mm$		
	0.25…5 for $\rho = 0.05mm$		

4.2 Application of artificial neural networks (ANN method)

With the help of Matlab's Neural Network Toolbox, an artificial neural network (ANN) was derived for each SCF. The data has been randomly divided into three subsets: 70 % training data, 15% validation data, and 15% testing data. The ANN is fitted to the training data. During training the validation set is used to measure network generalization and to stop training when generalization stops improving. Testing data has no effect on training of the ANN and is only used as independent measure for the network performance and quality of prognosis. Levenberg-Marquardt was chosen as training algorithm. The ANN feed-forward neural network consists of three hidden layers, where each hidden layer consists of 4 neurons according to the 4 input parameters (t_1, t_2, α, f_a). The output layer yields the stress concentration factor as output value ($\mathbf{k}_t = (K_{t,\,ANN})$). A graphical representation of the ANN is displayed in Fig. 4.

Each layer consists of a weight matrix $\mathbf{W}_i$, a bias $\mathbf{b}_i$, and a layer potential $\boldsymbol{\phi}_i$ which is transferred to a hyperbolic tangent sigmoid transfer function.

The restrictions to this method are similar to the PRC method in Table 7. More information on neural networks can be found in Hagan et al. [23].

Table 8 Stress concentration factors for equations applying to maximum principal stress according to new method

Loading	Sheet thickness t_1, t_2 [mm]	Radius ρ [mm]	Stress concentration factor
Tension	[0.25; 10]	0.05	$K^{f.p.}_{t,PRC,t,1}$
	[1.5; 20]	0.3	$K^{f.p.}_{t,PRC,t,2}$
	[5; 50]	1	$K^{f.p.}_{t,PRC,t,3}$
Bending	[0.25; 10]	0.05	$K^{f.p.}_{t,PRC,b,1}$
	[1.5; 20]	0.3	$K^{f.p.}_{t,PRC,b,2}$
	[5; 50]	1	$K^{f.p.}_{t,PRC,b,3}$

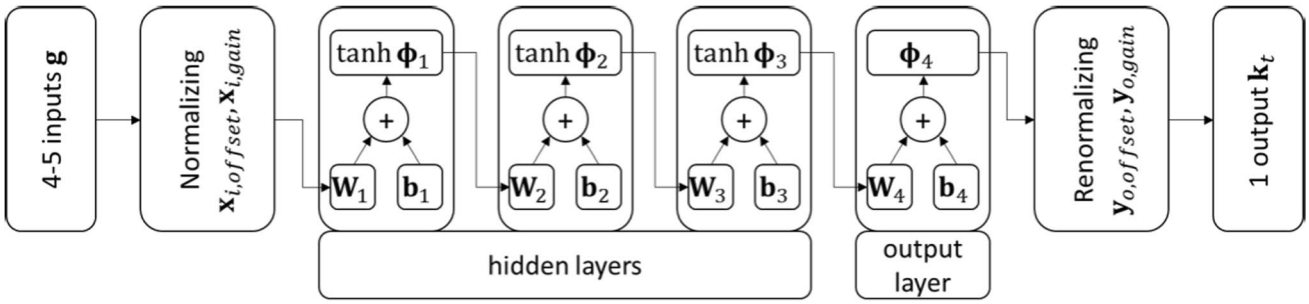

Fig. 4 Schematic structure of the artificial network

The multilayer approach with a low number of neurons in each hidden layer resulted in better estimation of stress concentration factors than a single-layer approach with a high number of neurons in the layer. Additionally, benefits in training and evaluation time could be accomplished.

The mathematical expressions for the used network can be found in Table 9[3], and the corresponding normalization vectors, weighting matrices, and bias vectors can be found in Tables 13, 14, 15, 16, 17 and 18.

5 Comparison of notch factor determination and quality

In order to draw a comparison between the aforementioned existing methods and the newly proposed methods using PRC and ANN, the given restrictions have to be kept in mind. In the following figures, the evaluated finite element results have been selected according to these restrictions.

It should be noted that:

– Keep in mind that the ratio of notch stress to structural stress $K_w = \sigma_n / \sigma_s$ has to meet a lower limit $K_{w,\,min}$; see Rother and Fricke [24]:

$$K_{w,\min} = 1.6 \text{ for } \rho = 1mm$$

$$K_{w,\min} = 2.13 \text{ for } \rho = 0.3mm$$

$$K_{w,\min} = 3.56 \text{ for } \rho = 0.05mm$$

[3] $\circ$ indicates the elementwise Hadamard product and $\oslash$ the elementwise Hadamard division.

In order to check K_w against the minimum ratio $K_{w,\,min}$, calculation of the structural stress is also required. This task has to be done by the user on top of the estimation of the SCF with the new equations.

5.1 Comparison of methods for T-joints

Figs. 5 and 6 show boxplots and probability plots for a normal distribution of the relative error which is calculated by:

$$err_{rel} = \frac{K_{t,EST} - K_{t,FEM}}{K_{t,FEM}} [\%] \tag{17}$$

Relative errors are calculated for all data points including training, validation, and testing data. The blue boxes in the boxplots show 50% of the data between the 25 and 75% quantiles. The distance between top and bottom of the blue box is the interquartile range. The red line is the median value. The black whiskers represent the last value within 1.5 times the interquartile range (the last value that is not an outlier) of the blue boxes.

Regarding the probability plots, the straight dashed lines represent a perfect normal distribution and are fitted to each data set.

Table 10 and 11 give additional statistical measures of the investigated data sets.

Table 9 Equations to be used for the ANN method

$\boldsymbol{\phi}_1 = \mathbf{b}_1 + \mathbf{W}_1 \cdot (((\mathbf{g} - \mathbf{x}_{i,\,offset}) \circ \mathbf{x}_{i,\,gain}) - \mathbf{1})$	(12)
$\boldsymbol{\phi}_2 = \mathbf{b}_2 + \mathbf{W}_2 \cdot \tanh(\boldsymbol{\phi}_1)$	(13)
$\boldsymbol{\phi}_3 = \mathbf{b}_3 + \mathbf{W}_3 \cdot \tanh(\boldsymbol{\phi}_2)$	(14)
$\boldsymbol{\phi}_4 = \mathbf{b}_4 + \mathbf{W}_4 \cdot \tanh(\boldsymbol{\phi}_3)$	(15)
$\mathbf{k}_t = ((\boldsymbol{\phi}_4 - \mathbf{y}_{o,\,offset}) \oslash \mathbf{y}_{o,\,gain}) - \mathbf{1}$	(16)

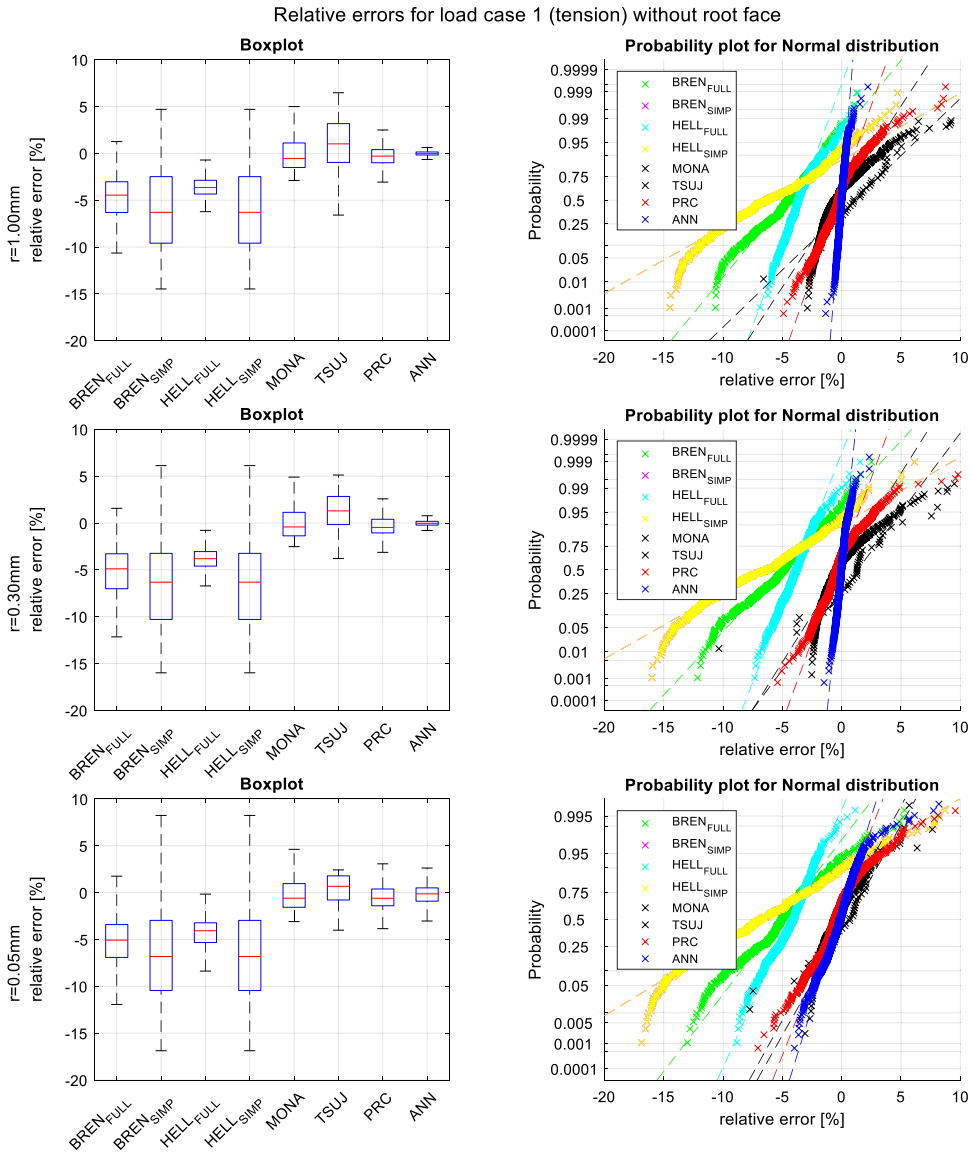

Fig. 5 Boxplot and probability plot of the relative errors for normal distribution—T-joint, load case 1 (tension)

Figs. 5 and 6 show the comparison of relative errors of each method for transverse non-load carrying stiffeners with fully penetrated welds (without root face). It should be noted that the methods by Brennan et al. and Hellier et al. have been derived with the assumption of plane stress condition which leads to a slight systematical deviation compared to PRC and ANN. The methods by Monahan and Tsuji tend remarkably well towards a median of little error. However, all these methods undergo multiple tight restrictions for the design variables. In consequence they can only be applied in comparison with a smaller subset of finite element computations; see the total numbers of used samples in Table 10 and 11. The PRC and ANN methods are capable of covering all evaluated finite element results and overall show improved performance in terms of significantly lower scattering around about zero or small relative error.

In terms of application of the newly introduced equations, the PRC method is slightly simpler to implement than the ANN method. The ANN will still yield more accurate predictions of SCFs. In order to reduce the computational effort for estimating SCFs for transverse non-load carrying stiffeners, the formulas for PRC and ANN will be provided via a programmed online solution which will be found in http://www.rother.userweb.mwn.de/scf-predictor.html [25].

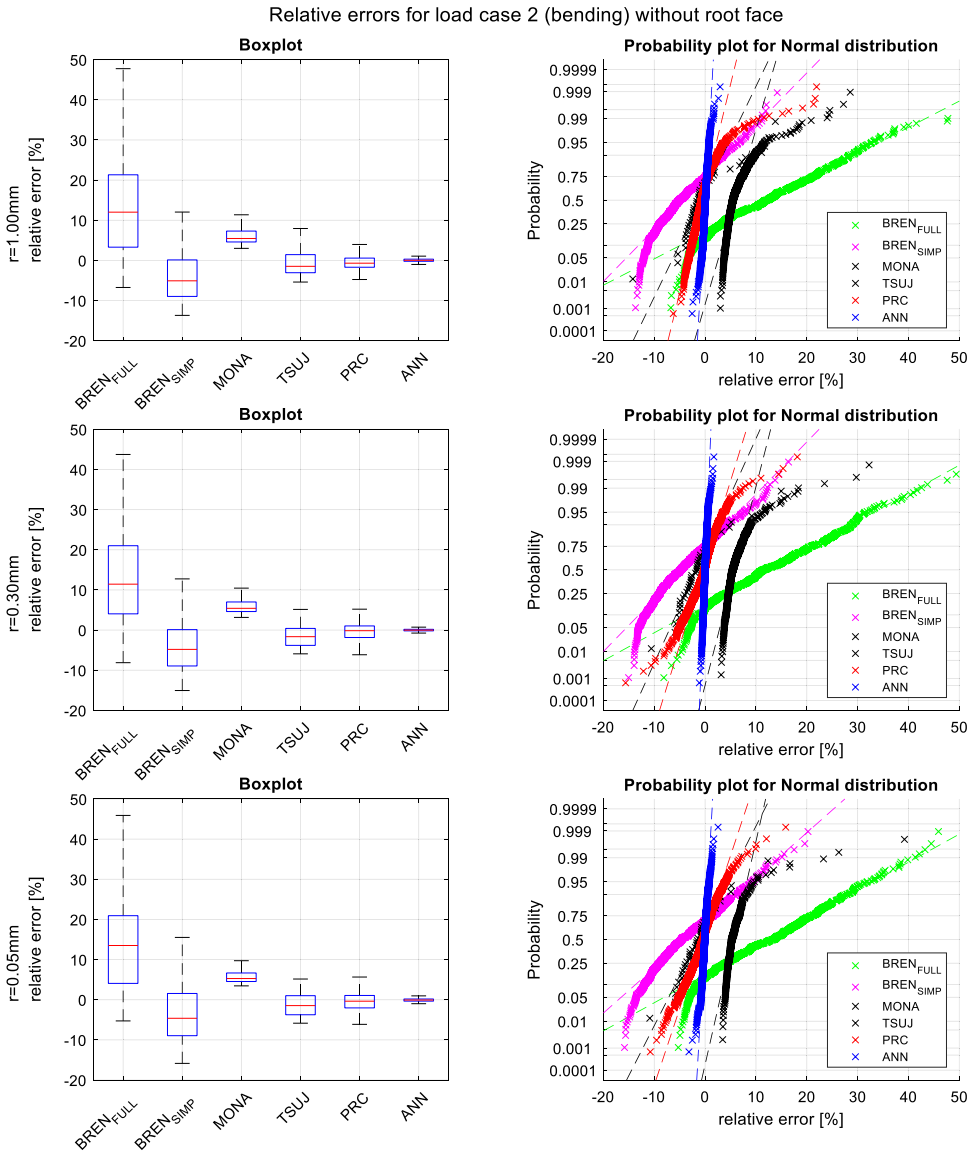

Fig. 6 Boxplot and probability plot of the relative errors for normal distribution—T-joint, load case 2 (bending)

Table 10 Statistical data of all evaluated parameter combinations, load case 1 (tension)

	Load case 1 (tension) without root face							
	$BREN_{FULL}$	$BREN_{SIMP}$	$HELL_{FULL}$	$HELL_{SIMP}$	MONA	TSUJ	PRC	ANN
Neglected results	39.62%	39.62%	39.62%	39.62%	54.53%	94.75%	3.6%	0%
Total number of used samples	1381	1381	1381	1381	1040	120	2204	2287
Mean	−4.98%	−6.46%	−3.88%	−6.46%	−0.04%	0.90%	−0.26%	−0.06%
Standard deviation	2.90%	4.72%	1.48%	4.72%	1.91%	2.79%	1.79%	0.80%
1% quantile	−11.68%	−15.79%	−7.84%	−15.79%	−2.59%	−8.53%	−4.28%	−2.62%
10% quantile	−9.06%	−12.78%	−5.73%	−12.78%	−2.01%	−2.49%	−2.13%	−0.76%
Median	−4.81%	−6.46%	−3.83%	−6.46%	−0.49%	−1.02%	−0.43%	−0.04%
90% quantile	−1.41%	−0.35%	−2.21%	−0.35%	3.02%	3.80%	1.84%	0.59%
99% quantile	1.75%	4.54%	0.07%	4.54%	9.10%	8.09%	5.18%	2.29%

Table 11 Statistical data of all evaluated parameter combinations, load case 2 (bending)

	Load case 2 (bending) without root face					
	$BREN_{FULL}$	$BREN_{SIMP}$	MONA	TSUJ	PRC	ANN
Neglected results	39.31%	39.31%	53.88%	94.76%	4.1%	0%
Total number of used samples	1391	1391	1057	120	2198	2292
Mean	12.86%	−4.02%	5.98%	−0.75%	−0.47%	0.004%
Standard deviation	11.02%	6.25%	2.04%	4.70%	2.34%	0.39%
1% quantile	−4.69%	−14.31%	3.45%	−11.88%	−7.16%	−1.29%
10% quantile	−1.67%	−11.53%	4.09%	−5.07%	−3.33%	−0.47%
Median	12.32%	−4.81%	5.40%	−1.58%	−0.44%	−0.01%
90% quantile	28.57%	4.58%	9.09%	5.97%	2.51%	0.51%
99% quantile	42.40%	12.23%	23.12%	14.16%	8.45%	1.30%

6 Conclusion

Existing estimations of SCFs at the weld toe of transverse non-load carrying stiffeners have been compared to two new estimations using PRC and ANN. The comparison has been drawn on the basis of FEAs with respect to the maximum principal stress in the weld toe assuming plane strain condition.

PRC and ANN not only increase the ranges of validity of existing SCF formulae but also show improved predictive quality which is shown by lower scattering of the relative errors.

The proposed methods may be incorporated into a programmed solution for the fast estimation of SCFs. The new methods will be programmed and made available for the community by http://rother.userweb.mwn.de/scf-predictor.html [25].

Appendix

Table 12 Regression formulae for PRC method for fully penetrated welds

k	f_k	c_k					
		$K^{f.p.}_{t,PRC,t,1}$	$K^{f.p.}_{t,PRC,t,2}$	$K^{f.p.}_{t,PRC,t,3}$	$K^{f.p.}_{t,PRC,b,1}$	$K^{f.p.}_{t,PRC,b,2}$	$K^{f.p.}_{t,PRC,b,3}$
1	1	−8.60483	−6.59428	−5.72123	−7.06393	−6.56684	−5.3789
2	α	0.154805	0.122145	0.107518	0.13486	0.121658	0.107623
3	t_1	1.55803	0.301566	0.100052	2.05336	0.408816	0.14865
4	f_a				2.19796	2.24764	
5	α^2	-0.000579344	−0.000454423	−0.000398838	−0.000512678	−0.000451622	−0.000413855
6	t_1^2	−0.060623	−0.0028683	−0.000386015	−0.0824741	−0.00425806	−0.000529817
7	f_a^2				−0.579303	−0.569353	
8	αt_1	−0.00624203	−0.00116491	−0.000368296	−0.00910366	−0.00174477	−0.0006289
9	αf_a				−0.0129674	−0.0131744	
10	$t_1 f_a$				0.146999	0.0307963	

Table 13 Neural network data for full penetration joints, tension loading, $\rho = 1.00mm$

$$x_{i,offset} = \begin{bmatrix} 110.02500 \\ 5.20250 \\ 5.51750 \\ 0.10280 \end{bmatrix} \qquad x_{i,gain} = \begin{bmatrix} 0.04004 \\ 0.04467 \\ 0.04498 \\ 2.51256 \end{bmatrix}$$

$$y_{o,\,offset} = 1.55949 \qquad y_{o,\,gain} = 1.14896$$

$$b_1 = \begin{bmatrix} -2.63750 \\ -1.52428 \\ -0.48874 \\ -0.30838 \\ -2.93238 \end{bmatrix} \qquad b_2 = \begin{bmatrix} 1.78577 \\ -1.20924 \\ -0.32212 \\ -1.14307 \\ -2.16028 \end{bmatrix} \qquad b_3 = \begin{bmatrix} 1.96254 \\ -0.71252 \\ -0.13066 \\ -0.48033 \\ 1.08610 \end{bmatrix} \qquad b_4 = -0.11368$$

$$W_1 = \begin{bmatrix} 0.12471 & -1.18246 & -0.04909 & 0.03565 \\ 1.22835 & 0.12309 & 0.00658 & 0.01149 \\ -0.00449 & 0.28566 & -0.46518 & -0.77593 \\ -0.03089 & -0.22904 & 0.01333 & 0.00489 \\ 0.09465 & -0.22888 & 0.63831 & 0.21563 \end{bmatrix}$$

$$W_2 = \begin{bmatrix} -0.41445 & 1.17610 & -0.78883 & -0.58004 & 0.38422 \\ 0.75332 & 0.43926 & 0.53550 & 0.79595 & 1.54875 \\ -1.16788 & 1.40932 & -0.16843 & -0.77458 & -1.16229 \\ -1.34748 & -0.63935 & -0.00848 & -1.02091 & 0.86437 \\ -0.49787 & -0.94745 & 1.33462 & 0.36518 & 0.35820 \end{bmatrix}$$

$$W_3 = \begin{bmatrix} -0.39408 & -1.05253 & 0.92820 & -0.99225 & 0.80445 \\ 0.49148 & -1.34799 & 1.32417 & -2.23282 & 0.50508 \\ -0.23179 & 0.61450 & 0.61442 & 0.96829 & -0.11020 \\ -0.06170 & -0.63832 & 1.63296 & 0.79919 & 0.46574 \\ 0.12877 & 0.96213 & 0.17480 & -0.91970 & -1.56047 \end{bmatrix}$$

$$W_4 = \begin{bmatrix} -0.14984 & -1.74079 & 1.67772 & 1.28830 & 1.20115 \end{bmatrix}$$

Table 14 Neural network data for full penetration joints, tension loading, $\rho = 0.30mm$

$$x_{i,offset} = \begin{bmatrix} 110.02500 \\ 1.62025 \\ 1.50925 \\ 0.10040 \end{bmatrix} \qquad x_{i,gain} = \begin{bmatrix} 0.04004 \\ 0.10887 \\ 0.10832 \\ 2.50250 \end{bmatrix}$$

$$y_{o,\,offset} = 1.64436 \qquad y_{o,\,gain} = 0.99020$$

$$b_1 = \begin{bmatrix} 2.13081 \\ -1.25447 \\ 0.12572 \\ 1.53450 \\ 3.03466 \end{bmatrix} \qquad b_2 = \begin{bmatrix} -2.03300 \\ 1.44868 \\ -0.29829 \\ 1.07395 \\ 1.23545 \end{bmatrix} \qquad b_3 = \begin{bmatrix} 1.88959 \\ 0.58858 \\ -0.05838 \\ -1.57365 \\ 2.03012 \end{bmatrix} \qquad b_4 = 0.65926$$

$$W_1 = \begin{bmatrix} -1.71847 & 0.30526 & -0.01004 & -0.03836 \\ 0.14315 & -0.99297 & -0.00813 & -0.00986 \\ 0.43550 & 0.08128 & -0.01607 & -0.02622 \\ 0.19476 & -1.16424 & 0.10822 & 0.07762 \\ -0.09295 & -0.87810 & 0.98216 & 1.60080 \end{bmatrix}$$

$$W_2 = \begin{bmatrix} 0.83447 & -1.31102 & -0.53128 & 0.58080 & -1.43636 \\ -0.87178 & 0.53373 & -0.40729 & -1.09208 & -0.10281 \\ -0.41707 & -1.03699 & 0.50613 & -0.36636 & 0.71042 \\ 0.88588 & -0.75765 & -0.39753 & -1.88193 & -1.02915 \\ 0.80325 & 0.09380 & -1.66384 & -0.21748 & -0.53330 \end{bmatrix}$$

$$W_3 = \begin{bmatrix} -1.06123 & -0.18605 & -2.00030 & -0.07764 & -1.29315 \\ -1.30634 & 0.96202 & -1.92346 & 0.20636 & -0.09881 \\ 0.29427 & -1.66571 & 0.20669 & 0.95220 & 0.92256 \\ -0.66960 & 0.29632 & -0.31867 & -0.94652 & 0.65731 \\ 0.51903 & 0.92214 & -1.04580 & 0.33136 & -0.63867 \end{bmatrix}$$

$$W_4 = \begin{bmatrix} -1.70759 & 0.62563 & -0.09762 & -1.10884 & -1.18112 \end{bmatrix}$$

Table 15 Neural network data for full penetration joints, tension loading, $\rho = 0.05mm$

$$x_{i,offset} = \begin{bmatrix} 110.02500 \\ 0.25238 \\ 0.25238 \\ 0.10040 \end{bmatrix} \qquad x_{i,gain} = \begin{bmatrix} 0.04004 \\ 0.42147 \\ 0.42232 \\ 2.50250 \end{bmatrix}$$

$$y_{o,\,offset} = 7.88860E-13 \qquad y_{o,\,gain} = 0.47092$$

$$b_1 = \begin{bmatrix} 1.38074 \\ 1.14626 \\ 0.25851 \\ -2.07276 \\ -1.35626 \end{bmatrix} \qquad b_2 = \begin{bmatrix} -1.91789 \\ -0.80858 \\ 0.19543 \\ -0.96326 \\ -2.12979 \end{bmatrix} \qquad b_3 = \begin{bmatrix} -1.96108 \\ -1.07827 \\ 0.18003 \\ 0.85566 \\ 2.04152 \end{bmatrix} \qquad b_4 = 0.69596$$

$$W_1 = \begin{bmatrix} -1.08722 & 0.13071 & -0.02262 & 0.00943 \\ -1.13488 & -1.36691 & -0.95868 & 0.51905 \\ 1.22694 & 0.37828 & -0.62815 & 1.34176 \\ -0.01705 & -1.16648 & -0.03054 & 0.07017 \\ -0.68938 & 1.29152 & -0.03971 & -0.00535 \end{bmatrix}$$

$$W_2 = \begin{bmatrix} 0.38829 & -0.05238 & 0.03802 & -1.31242 & 0.19868 \\ 1.61804 & 0.10663 & -0.14782 & 0.42953 & 0.74931 \\ 0.80894 & 0.36790 & -0.19685 & 1.00284 & -1.35807 \\ -0.52256 & 0.98236 & 0.44280 & 0.30795 & -1.08856 \\ -1.07802 & 0.07905 & -0.47301 & -0.69965 & 1.19837 \end{bmatrix}$$

$$W_3 = \begin{bmatrix} 1.30471 & -0.25925 & 0.65447 & -0.24550 & -1.20760 \\ 1.65298 & 0.00269 & 0.37120 & 0.36215 & -0.98153 \\ -1.31203 & -0.29506 & 0.03984 & 0.16727 & 0.81617 \\ 0.95156 & -1.12236 & -0.74351 & -0.54731 & -0.98864 \\ 1.02783 & 0.54741 & -0.52435 & -0.25411 & 0.80275 \end{bmatrix}$$

$$W_4 = \begin{bmatrix} 0.21386 & 0.90054 & -1.07093 & 0.64049 & -0.17511 \end{bmatrix}$$

Table 16 Neural network data for full penetration joints, bending loading, $\rho = 1.00mm$

$$x_{i,offset} = \begin{bmatrix} 110.02500 \\ 5.02250 \\ 5.02250 \\ 0.10040 \end{bmatrix} \qquad x_{i,gain} = \begin{bmatrix} 0.04016 \\ 0.04453 \\ 0.04449 \\ 2.50250 \end{bmatrix}$$

$$y_{o,\,offset} = 1.64973 \qquad y_{o,\,gain} = 0.80133$$

$$b_1 = \begin{bmatrix} 1.63277 \\ 2.41333 \\ -0.64862 \\ -1.15707 \\ 2.09145 \end{bmatrix} \qquad b_2 = \begin{bmatrix} -1.75421 \\ 0.26660 \\ 1.82541 \\ -1.04391 \\ 2.75519 \end{bmatrix} \qquad b_3 = \begin{bmatrix} -1.17615 \\ -0.98811 \\ -0.08376 \\ -0.73649 \\ 2.39243 \end{bmatrix} \qquad b_4 = 0.34003$$

$$W_1 = \begin{bmatrix} 0.14817 & 0.71954 & 0.01606 & -0.02038 \\ -2.24424 & 1.58089 & 0.23674 & -0.31005 \\ 0.29852 & 0.14528 & -0.00894 & 0.01092 \\ -0.00426 & 0.20859 & -0.01434 & 0.00999 \\ 0.23577 & -0.66331 & 0.93506 & 1.32037 \end{bmatrix}$$

$$W_2 = \begin{bmatrix} -0.69212 & 0.46098 & -0.89220 & -1.62336 & -0.43720 \\ -1.29039 & -0.06114 & 1.35085 & -1.92079 & 0.07900 \\ 0.69252 & -1.39025 & -1.30864 & -0.78577 & 0.31175 \\ -0.39087 & -1.10350 & 0.40069 & 1.09288 & 0.21067 \\ 0.92240 & 0.75467 & -0.90435 & -0.73245 & -0.32391 \end{bmatrix}$$

$$W_3 = \begin{bmatrix} 0.91787 & 2.13914 & -0.25659 & -0.18368 & 0.42503 \\ 0.97656 & -0.53693 & 0.64571 & -0.15607 & -1.36993 \\ -1.26038 & 1.92501 & -0.54514 & 1.14164 & 0.66525 \\ -1.00198 & -1.06328 & -0.47296 & 0.97266 & 0.94091 \\ 0.43214 & 0.33639 & 1.92539 & 0.57918 & 0.40035 \end{bmatrix}$$

$$W_4 = \begin{bmatrix} -1.14271 & 0.25950 & -0.53340 & 2.34893 & -0.04920 \end{bmatrix}$$

Table 17 Neural network data for full penetration joints, bending loading, $\rho = 0.30mm$

$$x_{i,offset} = \begin{bmatrix} 110.07500 \\ 1.69425 \\ 1.65725 \\ 0.10120 \end{bmatrix} \qquad x_{i,gain} = \begin{bmatrix} 0.04008 \\ 0.10964 \\ 0.10909 \\ 2.50501 \end{bmatrix}$$

$$y_{o,\,offset} = 1.70059 \qquad y_{o,\,gain} = 0.67532$$

$$b_1 = \begin{bmatrix} 2.07202 \\ -0.71703 \\ 0.86586 \\ 1.47502 \\ 1.74898 \end{bmatrix} \qquad b_2 = \begin{bmatrix} 1.70881 \\ -0.75112 \\ 0.32752 \\ -0.49243 \\ -1.89602 \end{bmatrix} \qquad b_3 = \begin{bmatrix} 1.77048 \\ -1.32134 \\ 0.24061 \\ -2.11095 \\ -1.58520 \end{bmatrix} \qquad b_4 = -0.91851$$

$$W_1 = \begin{bmatrix} -0.65933 & -0.28209 & -0.01241 & -0.14996 \\ 0.35745 & 0.03914 & 0.00299 & 0.01215 \\ 0.02481 & 0.31598 & 0.00294 & -0.00191 \\ 0.18557 & -0.33631 & 0.64000 & 0.64233 \\ 0.31851 & -0.68371 & 0.96568 & 0.35313 \end{bmatrix}$$

$$W_2 = \begin{bmatrix} -0.10760 & 0.56584 & -1.98384 & 2.23201 & -1.79552 \\ 1.21814 & -1.08944 & -1.24771 & -1.67719 & 0.97521 \\ -0.06392 & -0.80629 & -0.84312 & 1.21709 & -0.78558 \\ -0.43356 & -2.06808 & 0.33505 & -0.66776 & -0.30975 \\ -0.26405 & 0.42376 & -0.95184 & -1.07987 & -1.08719 \end{bmatrix}$$

$$W_3 = \begin{bmatrix} 0.52111 & 1.37444 & -0.93052 & -0.28999 & -0.10442 \\ 0.25004 & -0.74428 & -0.56135 & -0.59313 & -0.24936 \\ -1.49478 & -1.58103 & 2.08998 & -0.30687 & -0.19045 \\ 0.88150 & 2.14731 & 2.21917 & -1.74421 & 0.84367 \\ -1.66846 & -0.93697 & 1.89496 & 0.62419 & -0.27932 \end{bmatrix}$$

$$W_4 = \begin{bmatrix} -2.89344 & -1.48079 & 1.30095 & -1.34660 & 0.50663 \end{bmatrix}$$

Table 18 Neural network data for full penetration joints, bending loading, $\rho = 0.05mm$

$$x_{i,offset} = \begin{bmatrix} 110.02500 \\ 0.31412 \\ 0.27613 \\ 0.10040 \end{bmatrix} \qquad x_{i,gain} = \begin{bmatrix} 0.04004 \\ 0.42703 \\ 0.42445 \\ 2.50501 \end{bmatrix}$$

$$y_{o,\,offset} = 1.73216 \qquad y_{o,\,gain} = 0.52545$$

$$b_1 = \begin{bmatrix} -0.96940 \\ 1.89252 \\ -1.47518 \\ -0.43297 \\ -1.38961 \end{bmatrix} \qquad b_2 = \begin{bmatrix} -2.27294 \\ 0.26719 \\ -0.87922 \\ -0.03614 \\ 1.89663 \end{bmatrix} \qquad b_3 = \begin{bmatrix} -1.46064 \\ 0.26224 \\ 0.58167 \\ 0.22515 \\ -1.48161 \end{bmatrix} \qquad b_4 = -0.09216$$

$$W_1 = \begin{bmatrix} 0.37925 & 0.29004 & -0.00542 & 0.00711 \\ 0.14026 & 1.20831 & -0.00701 & 0.03851 \\ -0.14395 & -0.06946 & -0.36224 & -1.00100 \\ -0.09965 & 0.79746 & -0.02402 & -0.00040 \\ -0.09612 & -0.36752 & -0.10713 & -0.89858 \end{bmatrix}$$

$$W_2 = \begin{bmatrix} 0.08752 & -0.33646 & -1.00848 & 1.52606 & 0.22927 \\ -0.86555 & -1.37731 & 0.00143 & 0.94125 & -0.11690 \\ -0.78633 & 0.93987 & -2.03535 & 0.28000 & 2.04810 \\ 1.88640 & 1.16607 & -1.62983 & 0.87690 & 0.34264 \\ 1.85637 & -0.75186 & -0.67911 & -0.69471 & 0.63277 \end{bmatrix}$$

$$W_3 = \begin{bmatrix} 0.50921 & -0.72167 & 0.33727 & 0.04485 & 1.68031 \\ 0.40941 & 1.42415 & 0.69389 & 0.42211 & 1.44612 \\ -1.36562 & 0.40229 & -1.32157 & -0.37417 & 0.66370 \\ 2.19644 & 0.45524 & -0.15076 & 1.90735 & -0.58971 \\ -1.07089 & -0.18205 & -1.13850 & -0.31932 & 0.17478 \end{bmatrix}$$

$$W_4 = \begin{bmatrix} -0.47209 & -0.71701 & -1.31145 & 0.32785 & -1.07983 \end{bmatrix}$$

Acknowledgements The IGF project 19450 N of FOSTA - Forschungsvereinigung Stahlanwendung e. V., Düsseldorf, is funded by the Federal Ministry of Economic Affairs and Energy via the AiF within the framework of the program for the promotion of the Industrielle Gemeinschaftsforschung (IGF) based on a resolution of the German Bundestag. The financial support is greatly acknowledged.

Funding Open Access funding enabled and organized by Projekt DEAL.

Declarations

Conflict of interest The authors declare no competing interests.

Refernces

1. Hobbacher A, (2016) Recommendations for fatigue design of welded joints and components - IIW document IIW-2259-15 ex XIII-2460-13/XV-1440-13, Springer Verlag.
2. DVS - Deutscher Verband für Schweißen und verwandte Verfahren e. V (2017) Merkblatt DVS 0905 - Industrielle Anwendung des Kerbspannungskonzeptes für den Ermüdungsfestigkeitsnachweis von Schweißverbindungen. DVS Media GmbH, Düsseldorf
3. Baumgartner J, Hobbacher AF, Rennert R (2020) Fatigue assessment of welded thin sheets with the notch stress approach - Proposal for recommendations. Int J Fatigue 140:105844
4. Karakas Ö, Morgenstern C, Sonsino CM (2008) Fatigue design of welded joints from the wrought magnesium alloy AZ31 by the local stress concept with the fictitious notch radii of rf=1.0 and 0.05 mm. Int J Fatigue 30:2210–2219
5. Karakas Ö, Baumgartner J, Susmel L (2020) On the use of a fictitious notch radius equal to 0.3 mm to design against fatigue welded joints made of wrought magnesium alloy AZ31. Int J Fatigue 139:105747
6. Bruder T, Störzel K, Baumgartner J, Hanselka H (2012) Evaluation of nominal and local stress based approaches for the fatigue assessment of seam welds. Int J Fatigue 34:86–102
7. Köttgen VB, Olivier R and Seeger T, (1991) "Fatigue analysis of welded connections based on local stresses," in IIW XIII-1408-91.
8. Radaj D (1990) Design and analysis of fatigue resistant welded structures. Abington, Cambridge
9. Neuber H (1968) Über die Berücksichtigung der Spannungskonzentration bei Festigkeitsberechnungen. Konstruktion 20(7):245–251
10. Renken F, von Bock und Polach RUF, Schubnell J, Jung M, Oswald M, Rother K, Braun M (2021) An algorithm for statistical evaluation of weld toe geometries using laser triangulation. Int J Fatigue 149:106293
11. Alam MM, Barsoum Z, Jonsen P, Kaplan AFH, Häggblad HA (2010) The influence of surface geometry and topography on the fatigue cracking behaviour of laser hybrid welded eccentric fillet joints. Appl Surf Sci 256:1936–1945
12. Liinalampi S, Remes H, Lehto P, Lillemäe I, Romanoff J, Porter D (2016) Fatigue strength analysis of laser-hybrid welds in thin plate considering weld geometry in microscale. Int J Fatigue 87:143–152
13. Ottersböck MJ, Leitner M, Stoschka M (2021) Characterisation of actual weld geometry and stress concentration of butt welds exhibiting local undercuts. Eng Struct 240:112266
14. Oswald M, Rother K, Mayr C (2019) Determination of notch factors for welded cruciform joints based on numerical analysis and metamodeling. Weld World 63(5):1339–1354
15. Oswald M, Rother K, Neuhäusler J (2020) Determination of notch factors for welded butt joints based on numerical analysis and metamodeling. Weld World 64(3):2053–2074
16. Oswald M, Springl S and Rother K, (2020) "Determination of notch factors for welded T-joints based on numerical analysis and metamodeling," Int Inst Weld IIW-Doc-XIII-2853-2020.
17. Tsuji I (1990) Estimation of stress concentration factor at weld toe of non-load carrying fillet welded joints. West Jpn SocNaval Arch 80:241–251
18. Monahan CC, (1995) "Early fatigue crack growth at welds," Topics in Engineering. Comp Mech Publ 26.
19. Brennan FP, Peleties P, Hellier AK (2000) Predicting weld toe stress concentration factors for T and skewed T-joint plate connections. Int J Fatigue 22:573–584
20. Hellier AK, Brennan FP, Carr DG (2014) Weld Toe SCF and Stress Distribution Parametric Equations for Tension (Membrane) Loading. Adv Mater Res 891-892:1525–1153
21. Dabiri M, Ghafouri M, Rohani Raftar HR, Björk T (2017) Neural network-based assessment of the stress concentration factor in a T-welded joint. J Constr Steel Res 128:567–578
22. Sonsino CM (2009) Principles of local stress concepts for the assessment of welded joints. ESIS Newslett 45:30–34
23. Hagan MT, Demuth HB, M. Beale and O. De Jesus, Neural network design.
24. Rother K, Fricke W (2016) Effecitve notch stress approach for welds having low stress concentration. Int J Press Vessel Pip 147:12–20
25. Rother K, "SCF-Predictor," [Online]. Available: http://rother.userweb.mwn.de/scf-predictor.html. [Accessed 23 June 2021].
26. Leitner M, Stoschka M, Ottersböck M (2017) Fatigue assessment of welded and high frequency mechanical impact (HFMI) treated joints by master notch stress approach. Int J Fatigue 101:232–243
27. Schnabel K, Baumgartner J, Möller B (2019) Fatigue Assessment of Additively Manufactured Metallic Structures Using Local Approaches Based on Finite-Element Simulations. Proc Struct Integr 19:442–451
28. Hesseler J, Baumgartner J, Bleicher C (2021) Consideration of the transient material behavior under variable amplitude loading in the fatigue assessment of nodular cast iron using the strain-life approach. Fatigue Fract Eng Mater Struct 44:2845–2857. 1-13